International Journal of Scientific Research in Science and Technology
Print ISSN: 2395-6011 | Online ISSN: 2395-602X (www.ijsrst.com)
doi : https://doi.org/10.32628/IJSRST229653

Automatic Placement of Regions of Interest using Distance transform to Measure Spatial Resolution on the Clinical Computed Tomography Images : A Pilot Study

Ulil A. Taufiq, Choirul Anam*, Eko Hidayanto, Ariij Naufal

[1]Departement of Physics, Faculty of Science and Mathematics, Diponegoro University, Jl. Prof. Soedarto SH, Tembalang, Semarang 50275, Central Java, Indonesia.

*Corresponding author: anam@fisika.fsm.undip.ac.id

Article Info
Volume 9, Issue 6
Page Number : 462-471

Publication Issue
November-December-2022

Article History
Accepted : 01 Dec 2022
Published : 12 Dec 2022

ABSTRACT

We propose a new algorithm called distance transform region of interest (DT-ROI) to deal with the irregular patient's surface. The ROIs can be placed orthogonally along the patient's surface to get spatial resolution. The algorithm was developed using several image processing techniques. The original image was first segmented to obtain a segmented image. The segmented image was eroded and dilated to obtain an eroded and dilated image. Both the eroded and dilated images were edge detected to obtain the edge images of the eroded and dilated image. The edge images were distance transformed to obtain the closest pixel coordinate. Finally, ROIs were placed based on the coordinates obtained before. The DT-ROI was then assessed qualitatively by comparison with the ROI placement from the standard radial ROI (SR-ROI) on a Polymethyl methacrylate (PMMA) phantom, an anthropomorphic phantom, and the patient's computed tomography images. The algorithm resulted in orthogonalized ROIs, both along the irregular object and the circular object. The ROI comparison between DT-ROI and SR-ROI shows a little difference in terms of orthogonality on PMMA phantom. Meanwhile, on the anthropomorphic phantom and the patient's CT image, the DT-ROI produced a lot more orthogonal ROIs than the SR-ROI. Several ROIs of the DT-ROI have decreased orthogonality at certain sections, which can be observed in both phantom and patient images. However, theoretically, a slight decrease in orthogonality will not affect the modulation transfer function (MTF) measurement significantly. The DT-ROI algorithm has been successfully developed based on distance transformation and performed as the design. The algorithm can automatically place ROIs along the patient's irregular surface better than the SR-ROI algorithm. However, not all ROIs placed from DT-ROI are well-orthogonalized. DT-ROI still needs to be improved before it is used to

measure MTF to obtain a more optimal measurement.

Keywords: CT, distance transform, region of interest, orthogonality, spatial resolution

I. INTRODUCTION

Computed Tomography (CT) is a medical imaging modality producing excellent axial images using x-ray radiation. Based on the 2020/2021 United Nation Scientific Committee on The Effects of Atomic Radiation (UNSCEAR) report, CT examinations increased by 80% from the number reported in 2010. CT also contributed to the highest collective effective dose (61.6%), followed by conventional diagnostic radiology (23%), interventional radiology (8%), nuclear medicine diagnostics (7.2%), and dental radiology (0.2%) [1].

Examination using CT offers efficiency and effectiveness in obtaining quality images. One of the important image quality parameters is spatial resolution [2,3]. Generally, spatial resolution indicates the ability of the image to distinguish two or more small objects that are close together [3,4]. High resolution image provides more accurate information on small objects. It means the diagnosis will be more accurate as well.

Like other image quality parameters, spatial resolution has to be evaluated through quality control (QC) procedures [5]. Spatial resolution is generally evaluated by observing the bar pattern (BP) phantom visually [6]. However, this evaluation is rather qualitative because its accuracy is limited to the subjectivity of human observer. A more objective evaluation procedure is by developing a modulation transfer function (MTF) curve [7,8]. The MTF curve can be developed through the point spread function (PSF), line spread function (LSF) and edge spread function (ESF) [7,9,10]. The ESF is sometime used [11,12] because preparing edge targets is relatively easy and does not require special phantoms (microbead or wire phantoms) [9,13,14].

Spatial resolution of the CT system is generally obtained from a phantom image instead of patient [15,16]. However, measurements on the phantom cannot fully describe spatial resolution on patient image because it tends to describe the ideal capability of the imaging system in specific condition [17-20]. Therefore, measuring spatial resolution directly from patient image is an interesting prospect.

Up to date, the automation of image quality measurement to perform direct measurement on patient CT images has mostly focused on the noise parameters [19-23]. For spatial resolution, the related research is still limited due to some unresolved challenges [24,25].

One of the challenges to measuring a patient's spatial resolution, especially using the MTF curve, is the placement of the region of interests (ROI) at the edge. This is because of the irregular geometry comes from the patient's surface. It requires a more complex method to place the orthogonal ROI along the edge of the patient. Therefore, this study aims to automatically place the ROIs with sufficient orthogonality and match the contours of the surface of the object. In this paper, we offer a new method using the distance transform and the algorithm is called distance transform ROI (DT-ROI).

II. METHODS AND MATERIAL

A. DT-ROI algorithm development

The DT-ROI algorithm was developed using the Python programming. The algorithm was designed to be able to place orthogonalized ROIs along the surface

of the object based on the distance transform. DT is an image processing technique for changing a binary image consisting of a background and foreground into a new image with each pixel object having a value according to its minimum distance to the background [26-31]. The stages of DT-ROI development were consisting of segmentation, morphological operation (erosion and dilation), edge detection, distance transformation and ROI placement. Finally, the DT-ROI algorithm was assessed to know the quality of its ROI placement. The stages are shown in Figure 1.

The original image (Fig.1(a)) was segmented based on a threshold of -200 Hounsfield unit (HU). Segmentation on the original image produced a binary image which has the same shape to the original (Fig. 1b). The morphological operations used in this stage were dilation and erosion. Both dilation and erosion work by processing an image with a kernel (structuring element) [32,33].

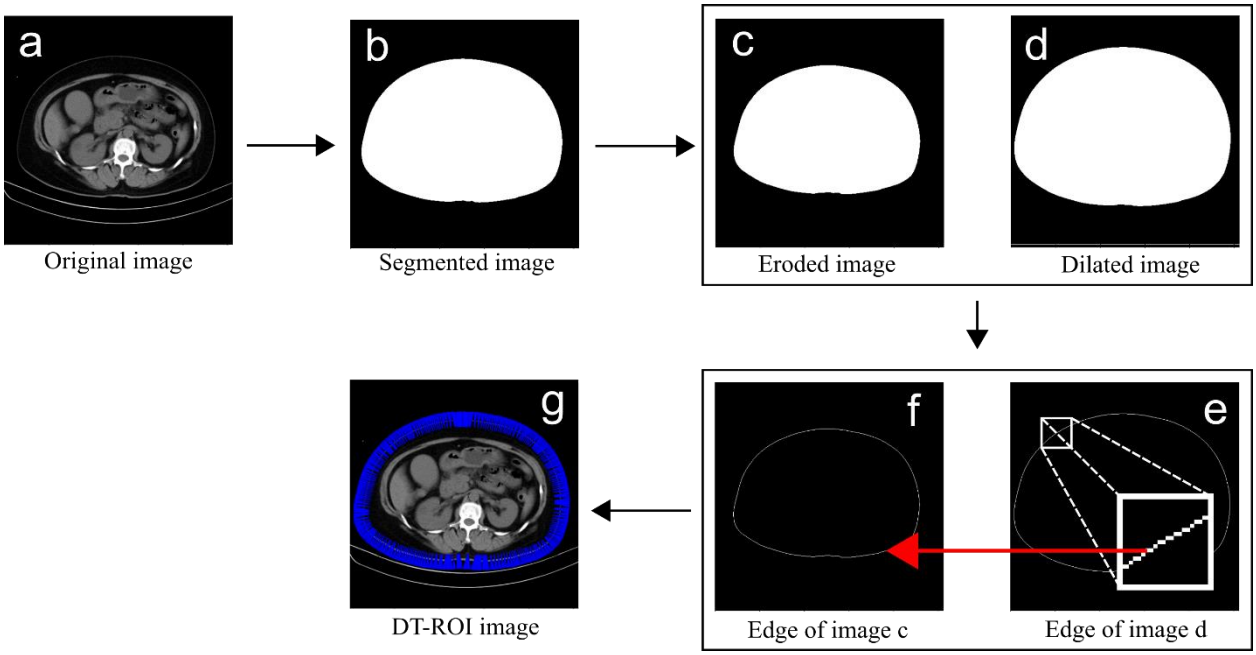

Figure 1. The DT-ROI development stages. (a) Original image, (b) Segmented image, (c) Dilated image, (d) Eroded image, (e) Edge of image d, (f) Edge of image c, and (g) DT-ROI image.

The segmented image (Fig.1(b)) from the segmentation operation was then eroded and dilated with disk kernel with radius of eight pixel (dk8) to obtain an eroded image (Fig.1(c)) and a dilated image (Fig.1(d)). The erosion and dilation operations were denoted by $c = b \ominus dk8$ and $d = b \oplus dk8$. The eroded and dilated images were then processed by edge detection. Edge detection obtained the edges of image d (Fig.1(e)) and the edge of image c (Fig.1(f)) for the next to be distance transformed to obtain the closest coordinate.

The distance transform was based on Euclidean Distance (ED) called the Euclidean Distance Transform (EDT) [28,30,34]. EDT was considered more accurate than other metrics in determining the shortest distance between two points (pixels) [26,35]. In general, the ED formulation of two points p and q is shown in Equations 1 or 2.

$$d(p,q) = \sqrt{\sum_{i=1}^{n}(p_i - q_i)^2} \quad (1)$$

or

$$d = \sqrt{(p_1 - q_1)^2 + (p_2 - q_2)^2 \ldots + (p_n - q_n)^2} \quad (2)$$

In particular, the ED of two points p and q in the two-dimensional is illustrated in Figure 2 and formulated in Equation 3. d is the distance between points p and q in two-dimensional coordinates p (p_x, p_y) and q (q_x, q_y). Δ_x and Δ_y are equal to $\Delta_x = p_x - q_x$ and $\Delta_y = p_y - q_y$.

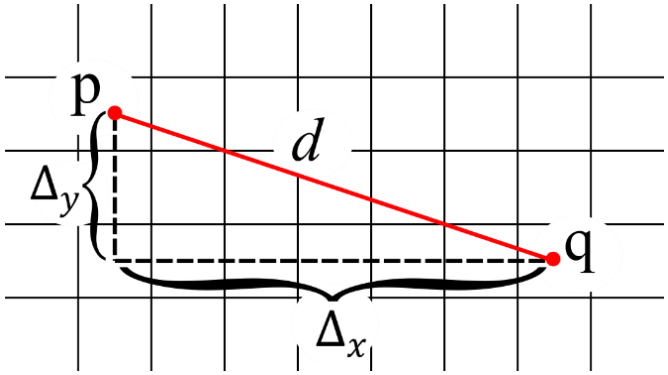

Figure 2. The Euclidean distance illustration in the two-dimensional.

$$d = \sqrt{(p_x - q_x)^2 + (p_y - q_y)^2} \quad (3)$$

In this distance transform stage, EDT was applied to each white pixel in the edge of image d (Fig.1(e)) towards the object in the edge of image c (Fig.1(f)). The EDT process produced the closest distance value between each white pixel on the edge of image d (Fig.1(e)) and the edge object on the edge of image c (Fig.1(f)). This process also produced the coordinate of closest pixel.

The ROI shape for measuring MTF at the edges was 2D profile line. Using the coordinates returned from white pixel in the edge of image d and returned from the EDT, the line ROIs were placed by connecting the line through the two coordinates. The ROIs were then overlaid on the original image to create the DT-ROI image (Fig.1(g)) and displayed in the figure window for observation.

B. ROIs quality assessment

ROIs were assessed from its orthogonality to the surface of the object. Higher orthogonality meant better because the MTF measurement requires high orthogonality in order to obtain optimal values [36-41]. In this study, the ROIs orthogonality of DT-ROI was assessed qualitatively by comparing the ROIs placement from DT-ROI with the ROIs placement from standard radial ROI (SR-ROI) on a Polymethyl methacrylate (PMMA) phantom, an anthropomorphic phantom, and a patient CT image. The PMMA phantom was used to assess ROIs placement on circular surfaces, while the anthropomorphic phantom and CT image of the patient were used to assess ROIs placement on irregular surfaces.

SR-ROI was chosen as benchmark in this study because of its specialization. SR-ROI was part of an algorithm developed by Ainurrofik et al. (2021) [10] that is able to place ROI based on the radial method, resulting in ROIs with high orthogonality only on objects with circular surfaces.

III.RESULTS AND DISCUSSION

The DT-ROI algorithm has been successfully developed according to the design. The algorithm is able to automatically place orthogonalized ROI along the irregular object surface (patient). Figure 3 shows the ROIs placed by DT on abdominal image.

The comparison between the DT and SR-ROI on a circular PMMA phantom is shown in Figure 4. SR-ROI (Fig.4(b)) places ROI with higher orthogonality than DT-ROI (Fig.4(a)). ROIs placement in DT-ROI, there are several ROIs that are not well-orthogonalized.

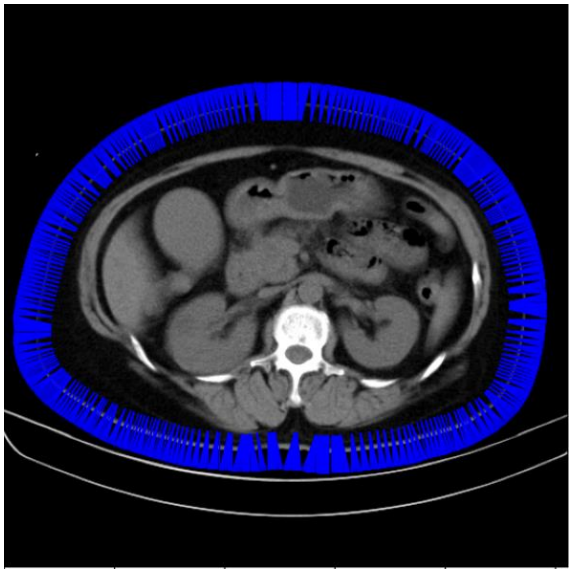

Figure 3. ROIs placement using the DT-ROI algorithm on patient CT image.

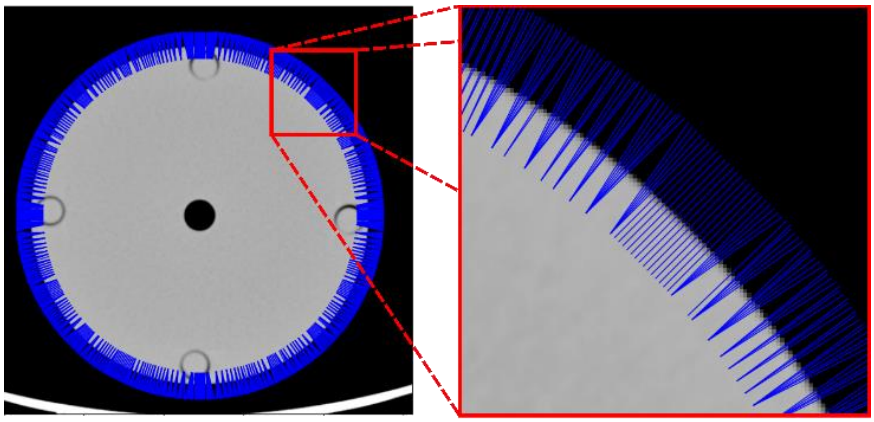

(a)

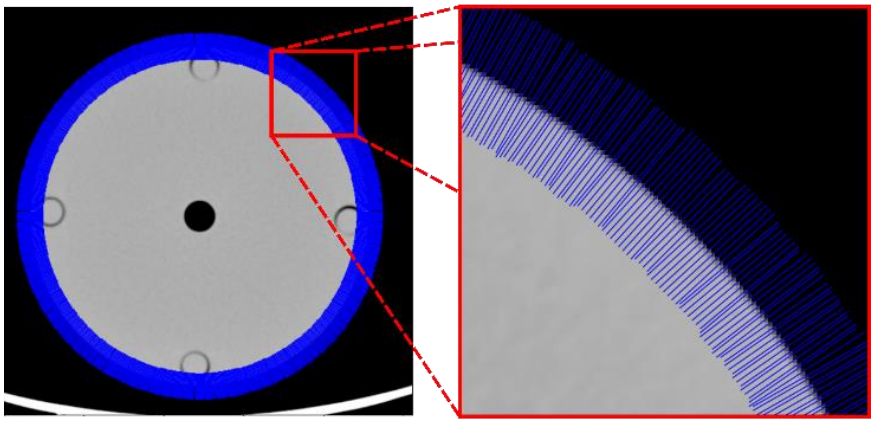

(b)

Figure 4. ROIs placement on a PMMA phantom. (a) ROIs placement using DT-ROI and (b) ROIs placement on using SR-ROI.

Comparison between the DT-ROI and SR-ROI algorithms on an anthropomorphic phantom (irregular surfaced object) is shown in Figure 5. DT-ROI (Fig.5(a)) clearly places ROs with higher orthogonality than SR-ROI (Fig.5(b)). SR-ROI shows significantly lower ROIs orthogonality at high

curvature sections. The decrease in the orthogonality occurs because the SR-ROI is not suitable to be applied to irregular phantoms. SR-ROI is designed specifically for standard phantom with circular shape [10].

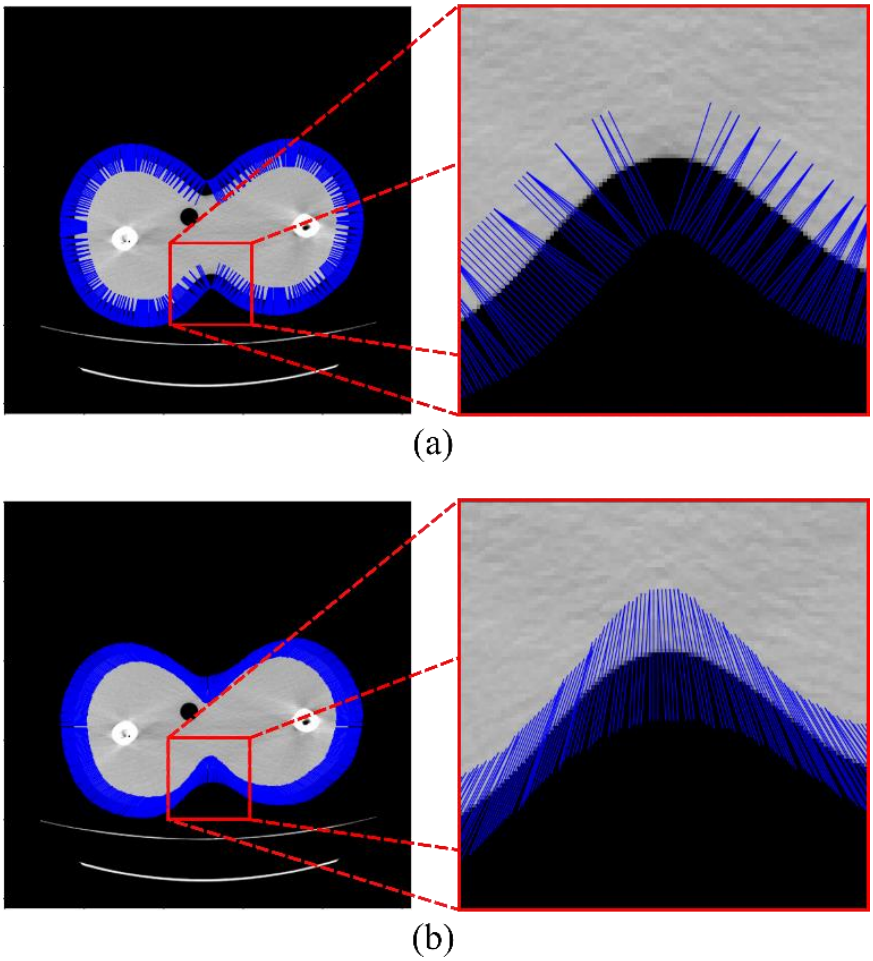

Figure 5. ROIs placement on an Anthropomorphic phantom (pelvis area). (a) ROIs placement using DT-ROI and (b) ROIs placement using SR-ROI

A similar case can also be observed in ROIs placement of a patient's CT image (irregular surfaced object) as shown in Figure 6. DT-ROI (Fig.6(a)) also places higher orthogonality than SR-ROI (Fig.6(b)) for the same reason. SR-ROI shows lower orthogonality on the left side of the zoom panel in Figure 5b.

Some of the ROIs that are not well-orthogonalized in DT-ROI occurs in all applications. This happens because of a mismatch in the morphological operation stage, especially in the kernel model. The mismatch from using the kernel model causes the EDT operation to produce the closest pixel coordinates that assemble at one point, so that the ROI placement has low orthogonality in that part. However, the decrease in ROI orthogonality occurring in DT-ROI is relatively low. That means it will not significantly affect the value of MTF measurements later, as in previous studies on MTF measurements of slanted edges [36,40,41].

IV. CONCLUSION

The proposed algorithm, namely DT-ROI, has been successfully developed according to the design. The DT-ROI can automatically place the ROIs orthogonally along the irregular patient's surface. The ROI placement of DT-ROI on patient's is better than SR-ROI. However, there are several ROIs that are not well-orthogonalized in the DT-ROI. This problem needs to be solved before the algorithm is used to

measure the MTF so that the DT-ROI can obtain a more optimal measurement.

V. ACKNOWLEDGEMENTS

This work was funded by the Riset Publikasi International Bereputasi Tinggi (RPIBT), Diponegoro University, No. 569-187/UN7.D2/PP/VII/2022.

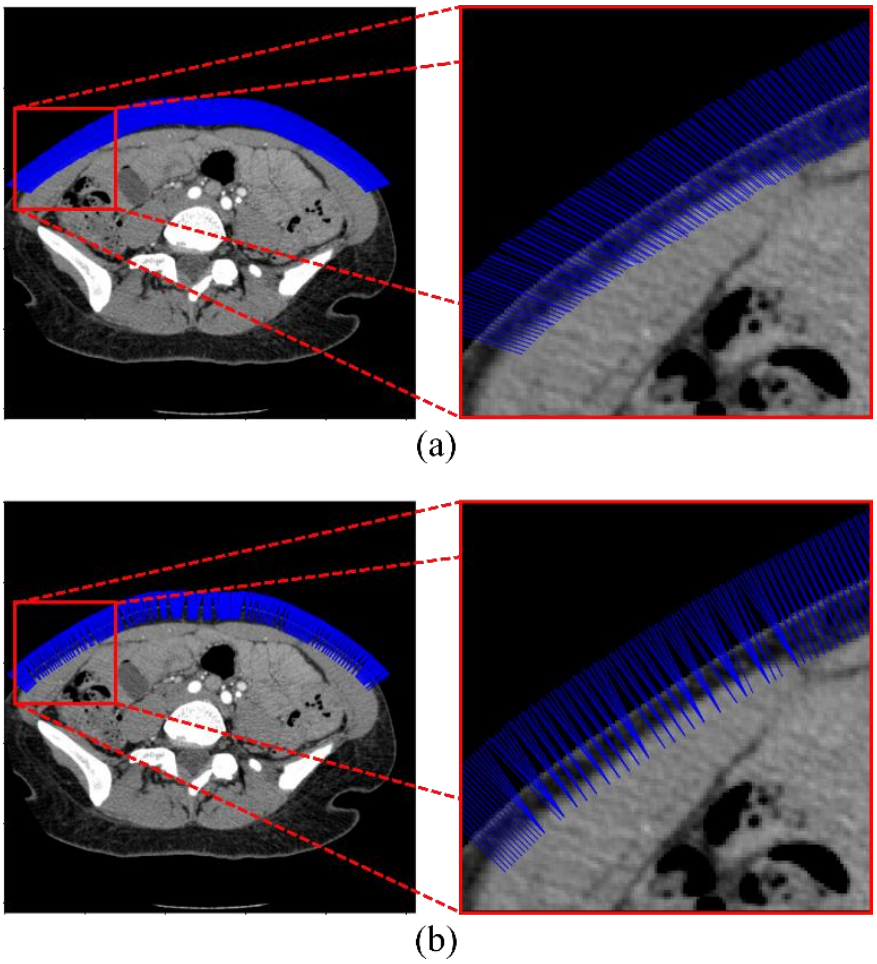

Figure 6. ROI placement on a patient's CT image (abdomen). (a) ROI placement using DT-ROI and (b) ROI placement using SR-ROI.

VI. REFERENCES

[1] United Nations Scientific Committee on the Effects of Atomic Radiation. Sources, Effects and Risks of Ionizing Radiation, United Nations Scientific Committee on the Effects of Atomic Radiation (UNSCEAR) 2020/2021 Report, Volume I: Report to the General Assembly, with Scientific Annex A-Evaluation of Medical Exposure to Ionizing Radiation. United Nations; 2022.

[2] Pauwels R, Silkosessak O, Jacobs R, Bogaerts R, Bosmans H, Panmekiate S. A pragmatic approach to determine the optimal kvp in cone beam CT: Balancing contrast-to-noise ratio and radiation dose. *Dentomaxillofacial Radiology*. 2014;43(5):20140059.

[3] Gascho D, Thali MJ, & Niemann T. Post-mortem computed tomography: technical principles and recommended parameter settings for high-resolution imaging. *Medicine, Science and the Law*. 2018;58(1):70-82.

[4] Tolentino EdeS, Amoroso-Silva PA, Alcalde MP, et al. Accuracy of high-resolution small-volume cone-beam computed tomography in detecting complex anatomy of the apical isthmi: ex vivo analysis. *Journal of Endodontics*. 2018;44(12):1862-1866.

[5] INTERNATIONAL ATOMIC ENERGY AGENCY. Quality Assurance Programme for Computed Tomography: Diagnostic and Therapy Applications. In IAEA Human Health Series No. 19. IAEA: Vienna. 2012.

[6] González-López A, Campos-Morcillo PA, & Lago-Martín JD. An oversampling procedure to calculate the MTF of an imaging system from a bar-pattern image. *Medical Physics*. 2016:43(10);5653-5658.

[7] Anam C, Fujibuchi T, Budi WS, Haryanto F, Dougherty G. An algorithm for automated modulation transfer function measurement using an edge of a PMMA phantom: Impact of field of view on spatial resolution of CT images. *Journal of Applied Clinical Medical Physics*. 2018:19(6);244-252.

[8] Rueckel J, Stockmar M, Pfeiffer F, Herzen J. Spatial resolution characterization of a X-ray microCT system. *Applied Radiation and Isotopes*. 2014;94:230-234.

[9] Manson EN, Bambara L, Nyaaba RA, et al. Comparison of Modulation Transfer Function Measurements for Assessing The Performance of Imaging Systems. *Medical Physics*. 2017;5(2):188-191.

[10] Ainurrofik N, Anam C, Sutanto H, Dougherty G. An automation of radial modulation transfer function (MTF) measurement on a head polymethyl methacrylate (PMMA) phantom. *AIP Conference Proceedings*. 2021;2346 (1):040009.

[11] González-López A. Effect of noise on MTF calculations using different phantoms. *Medical Physics*. 2018;45(5):1889-1898.

[12] Maruyama S. Assessment of Uncertainty Depending on Various Conditions in Modulation Transfer Function Calculation Using the Edge Method. *J Med Phys*. 2021;46(3):221-227.

[13] Kayugawa A, Ohkubo M, & Wada S. Accurate determination of CT point-spread-function with high precision. *Journal of Applied Clinical Medical Physics*. 2013;14(4):216-226.

[14] Xie X, Fan H, Wang A, Zou N, & Zhang Y. Regularized slanted-edge method for measuring the modulation transfer function of imaging systems. *Applied optics*. 2018;57(22):6552-6558.

[15] Brunner CC, Stern SH, Minniti R, Parry MI, Skopec M, & Chakrabarti K. CT head-scan dosimetry in an anthropomorphic phantom and associated measurement of ACR accreditation-phantom imaging metrics under clinically representative scan conditions. *Medical Physics*. 2013;40(8):081917.

[16] Bor D, Unal E, & Uslu A. Comparison of different phantoms used in digital diagnostic imaging. *Nuclear Instruments and Methods in Physics Research Section A: Accelerators, Spectrometers, Detectors and Associated Equipment*. 2015;795:160-166.

[17] Gay F, Pavia Y, Pierrat N, Lasalle S, Neuenschwander S, & Brisse HJ. Dose reduction with adaptive statistical iterative reconstruction for paediatric CT: phantom study and clinical experience on chest and abdomen CT. *European Radiology*. 2014;24(1):102-111.

[18] Cheng Y, Abadi E, Smith TB, et al. Validation of algorithmic CT image quality metrics with preferences of radiologists. *Medical Physics*. 2019;46(11):4837-4846.

[19] Ahmad M, Jacobsen MC, Thomas MA, Chen HS, Layman RR, & Jones AK. A Benchmark for automatic noise measurement in clinical computed tomography. *Medical Physics*. 2021;48(2):640-647.

[20] Chun M, Choi JH, Kim S, Ahn C, & Kim JH. Fully automated image quality evaluation on patient CT: Multi-vendor and multi-

reconstruction study. *PloS one*. 2022;17(7):e0271724.

[21] Christianson O, Winslow J, Frush DP, Samei E. Automated Technique to Measure Noise in Clinical CT Examinations. *AJR Am J Roentgenol*. 2015;205(1):W93-W99.

[22] Malkus A, Szczykutowicz TP. A method to extract image noise level from patient images in CT. *Medical Physics*. 2017;44(6):2173-2184.

[23] Anam C, Budi WS, Fujibuchi T, Haryanto F, & Dougherty G. Validation of the tail replacement method in MTF calculations using the homogeneous and non-homogeneous edges of a phantom. *Journal of Physics: Conference Series*. 2019;1248(1):012001.

[24] Li K, Garrett J, Ge Y, & Chen GH. Statistical model based iterative reconstruction (MBIR) in clinical CT systems. Part II. Experimental assessment of spatial resolution performance. *Medical physics*. 2014;41(7):071911.

[25] Sanders J, Hurwitz L, & Samei E. Patient-specific quantification of image quality: an automated method for measuring spatial resolution in clinical CT images. *Medical Physics*. 2016;43(10):5330-5338.

[26] Shih FY. *Image processing and mathematical morphology: fundamentals and applications*. CRC Press; 2017.

[27] Li F, Zlatanova S, Koopman M, Bai X, & Diakité A. Universal path planning for an indoor drone. *Automation in Construction*. 2018;95:275-283.

[28] Baum D, Weaver JC, Zlotnikov I, Knötel D, Tomholt L, & Dean MN. High-throughput segmentation of tiled biological structures using random-walk distance transforms. *Integrative and Comparative Biology*. 2019;59(6):1700-1712.

[29] Elizondo-Leal JC, Ramirez-Torres JG, Barrón-Zambrano JH, Diaz-Manríquez A, Nuño-Maganda MA, & Saldivar-Alonso VP. Parallel raster scan for Euclidean distance transform. *Symmetry*. 2020;12(11):1808.

[30] Marasca A, Backes A, Favarim F, Teixeira M, & Casanova D. EDT method for multiple labelled objects subject to tied distances. *International Journal of Automation and Computing*. 2021;18(3):468-479.

[31] Wang J, & Tan Y. Efficient Euclidean distance transform algorithm of binary images in arbitrary dimensions. *Pattern Recognition*. 2013;46(1):230-242.

[32] Abdalla M, & Nagy B. Dilation and erosion on the triangular tessellation: an independent approach. *IEEE Access*. 2018;6:23108-23119.

[33] Deng L, Zhang J, Xu G, & Zhu H. Infrared small target detection via adaptive M-estimator ring top-hat transformation. *Pattern Recognition*. 2021;112:107729.

[34] Fuseiller G, Marie R, Mourioux G, Duno E, & Labbani-Igbida O. Enhancing distance transform computation by leveraging the discrete nature of images. *Journal of Real-Time Image Processing*. 2022;19:763-773.

[35] Akkoul S, Hafiane A, Rozenbaum O, Lespessailles E, & Jennane R. 3D Reconstruction of the proximal femur shape from few pairs of x-ray radiographs. *Signal Processing: Image Communication*. 2017;59:65-72.

[36] Xie X, Fan H, Wang H, Wang Z, & Zou N. Error of the slanted edge method for measuring the modulation transfer function of imaging systems. *Applied Optics*. 2018;57(7):B83-B91.

[37] Narita A, Ohkubo M, Fukaya T, & Noto Y. A simple method for measuring the slice sensitivity profile of iteratively reconstructed CT images using a non-slanted edge plane. *Medical Physics*. 2021;48(3):1125-1130.

[38] Kajihara Y, Fukuzawa K, Itoh S, Watanabe R, & Zhang H. Theoretical and experimental study on two-stage-imaging microscopy using ellipsometric contrast for real-time visualization of molecularly thin films. *Review of Scientific Instruments*. 2013;84(5):053704.

[39] Tsai YW, Chu CH, Shih WH, Jin SC, Chen JC, & Liang,KC. Evaluation of different modulation transfer function measurement based on different edge spread function calculations. *Journal of Medical and Biological Engineering*. 2019;39(6):901-911.

[40] Xiang C, Chen X, Chen Y, Zhou J, & Shen W. MTF measurement and imaging quality evaluation of digital camera with slanted-edge method. *Optical Design and Testing IV*. 2010;7849:85-92.

[41] Estribeau M, & Magnan P. Fast MTF measurement of CMOS imagers using ISO 12333 slanted-edge methodology. *Detectors and Associated Signal Processing*. 2004;5251:243-252.

Cite this article as :

Ulil A. Taufiq, Choirul Anam, Eko Hidayanto, Ariij Naufal, "Automatic Placement of Regions of Interest using Distance transform to Measure Spatial Resolution on the Clinical Computed Tomography Images : A Pilot Study", International Journal of Scientific Research in Science and Technology (IJSRST), Online ISSN : 2395-602X, Print ISSN : 2395-6011, Volume 9 Issue 6, pp. 462-471, November-December 2022. Available at doi : https://doi.org/10.32628/IJSRST229653
Journal URL : https://ijsrst.com/IJSRST229653